Bulletin of Mathematical Biology (2006) 68: 1975–2003
DOI 10.1007/s11538-006-9060-5

ORIGINAL ARTICLE

Interactions Between Pattern Formation and Domain Growth

A.A. Neville, P.C. Matthews, H.M. Byrne*

Centre for Mathematical Medicine, School of Mathematical Sciences, University of Nottingham, Nottingham NG7 2RD, UK

Received: 3 June 2005 / Accepted: 28 November 2005 / Published online: 20 May 2006

Abstract In this paper we develop a theoretical framework for investigating pattern formation in biological systems for which the tissue on which the spatial pattern resides is growing at a rate which is itself regulated by the diffusible chemicals that establish the spatial pattern. We present numerical simulations for two cases of interest, namely exponential domain growth and chemically controlled growth. Our analysis reveals that for domains undergoing rapid exponential growth dilution effects associated with domain growth influence both the spatial patterns that emerge and the concentration of chemicals present in the domain. In the latter case, there is complex interplay between the effects of the chemicals on the domain size and the influence of the domain size on the formation of patterns. The nature of these interactions is revealed by a weakly nonlinear analysis of the full system. This yields a pair of nonlinear equations for the amplitude of the spatial pattern and the domain size. The domain is found to grow (or shrink) at a rate that depends quadratically on the pattern amplitude, the particular functional forms used to model the local tissue growth rate and the kinetics of the two diffusible species dictating the resulting behaviour.

Keywords Pattern formation · Reaction-diffusion · Domain growth · Weakly nonlinear analysis

1. Introduction

Since Alan Turing (1952) first proposed reaction-diffusion (RD) theory to describe the range of spatial patterns observed in the developing embryo, RD models have been studied extensively (Maini et al., 1997; Murray, 1993; Neubert et al., 2002; Ouyang and Swinney, 1991; Painter et al., 1999). For example, Lengyel and Epstein (1991) proposed a mathematical model for the first chemical reaction, the

*Corresponding author.
E-mail address: Helen.Byrne@nottingham.ac.uk (H.M. Byrne).

chlorite-iodide-malonic acid starch (CIMA) reaction, known to exhibit Turing patterns and Painter et al. (2000) developed a RD model that reproduced some of the complex patterns observed on the skin of certain animals. Other authors, also motivated by pattern formation during animal coat development, have proposed RD models that incorporate domain growth (Varea et al., 1997). For example, Kondo and Asai (1995) investigated the formation of stripes on the marine angelfish *Pomacanthus* by simulating a RD wave on a one-dimensional array of cells, increasing the domain size during computation to account for growth. They observed good agreement between the real and simulated pattern arrangements. However, most existing models of pattern formation on growing domains do not couple tissue growth with the chemical concentrations within the domain. As such they provide only limited insight into the following question that was posed by Harrison and Kolář (1988); 'How are the actions of morphogens coordinated with the process of growth?' Certainly, there are biological systems for which domain growth is independent of the chemicals present. These include the development of coat patterns on mammals and the patterning of butterfly wings (Murray, 1993). However, in certain situations the coupling of domain growth to the chemicals present is likely to be important (Alberts et al., 1994). For example, a major factor in the failure of a significant number of vascular reconstructions is the unscheduled proliferation of vascular smooth muscle cells. Such tissue growth may be stimulated by a variety of growth factors, including platelet-derived growth factor, but inhibited by others, such as transforming growth factor-β (Majack, 1987). Also a large number of chemicals may influence tumour development (Alberts et al., 1994), such as transforming growth factor-α which is thought to contribute to the growth of glioblastomas but drugs, such as Tamoxifen, can suppress such tissue growth (Campbell and Pollack, 1997).

There have been numerous mathematical models proposed which are concerned with tumour biology (Byrne and Chaplain, 1995; Casciari et al., 1992; Chaplain, 1996; Sherratt and Chaplain, 2001; Ward and King, 1997). Chaplain et al. (2001) used reaction-diffusion theory to examine spatio-temporal pattern formation on the surface of a tumour spheroid. The position of the tumour boundary was assumed to grow linearly in time. Their numerical results were in good agreement with in vitro experiments, with proliferative heterogeneity of cancer cells being observed in solid tumours at all stages of development. Other authors to investigate spatio-temporal patterning during tumour growth are Owen and Sherratt (1999), who pay particular attention to the influx of macrophages (types of white blood cell that form part of the body's immune response system) into a small avascular tumour. They discovered the existence of travelling wave solutions, where the wave front is taken as a moving boundary, and showed that, in the context of tumour–macrophage interactions, spatial variations may arise as a consequence of differential cell movement and chemical diffusion. When macrophage chemotaxis was also included in the model, a qualitatively new type of behaviour could be observed, namely irregular spatio-temporal oscillations behind the wave front. Earlier, more general models of tumour growth, which do not consider pattern formation explicitly, include the work of Greenspan (1976), wherein cellular material moves as a result of internal pressure differentials, which arise from cell birth and death.

In this paper we combine ideas developed in the papers mentioned above (Byrne and Chaplain, 1995; Casciari et al., 1992; Chaplain, 1996; Chaplain et al., 2001; Greenspan, 1976; Owen and Sherratt, 1999; Sherratt and Chaplain, 2001; Ward and King, 1997) to develop a general theoretical framework for studying pattern formation within a growing domain, where the domain represents a generic tissue. (We note that this generality lies in allowing a large class of growth dependencies to obtain the same amplitude equations for the mentioned pattern types.) Cell birth and death within the tissue generate a velocity field that controls the rate of domain growth. We assume that there are two interacting diffusible chemicals within the domain and investigate the ability of the system to generate spatial patterns for different choices of the net rate of cell proliferation (and hence domain growth). We show that if the local growth rate is constant and, hence, independent of the chemicals present, then domain growth is exponential and, in doing so, recover the model developed by Crampin et al. (1999). They considered a RD model on a slowly and isotropically growing domain and showed, via numerical simulation and a self-similarity argument, that a frequency-doubling sequence of patterns could be generated.

Most models of chemically controlled growth focus on a single, growth-rate limiting diffusible species (Breward et al., 2002; Byrne and Chaplain, 1998; Ward and King, 1997). As far as we are aware, Crampin et al. (2002) are unique in studying domain growth that is influenced by two chemical species. First, they considered nonuniform growth by splitting a one-dimensional domain into two sub-regions, each undergoing slow, uniform growth, with a different strain rate (specifying the local growth characteristics) and reactant concentrations and their fluxes being continuous at the moving interface permitting communication between the two regions. They then considered briefly a case for which domain growth was dependent on the activating chemical in the domain. Although their model is similar to the one that we develop, unlike us the authors did not perform a mathematical analysis of their system, focussing instead on numerical solutions.

While numerical simulations of Turing systems are useful for correctly predicting pattern formation, it is often difficult to explain the resulting patterns. In this paper, we use weakly nonlinear analysis to construct approximate model solutions and, in so doing, explain how interactions between the chemicals and the changing domain lead to the range of behaviour revealed by our numerical simulations. Weakly nonlinear analysis has been used by other authors (Benson et al., 1998, 1993; Grindrod, 1996) to study Turing systems and has shown that RD mechanisms have a greater potential for generating spatial patterns than linear analysis of standard Turing systems might suggest.

The remainder of this paper is organised as follows. In Section 2 we formulate our model for pattern formation in a RD system in which domain growth may be influenced by the local concentration of the reacting chemicals. Numerical results are given in Section 3 for the cases of exponential and chemically controlled domain growth. In Section 4 we use weakly nonlinear analysis to derive and analyse nonlinear equations that describe the interactions between the amplitude of the spatial patterns and the growth of the domain. The paper concludes in Section 5 with a summary and discussion of the key results.

2. Model formulation

In this section, we develop our model of pattern formation within a growing tissue. We assume that the domain represents a generic tissue which receives nutrients and eliminates waste products via reaction and diffusion only. The tissue consists of live cells and volume changes associated with cell birth and death generate a velocity field that drives domain growth (Alison and Sarraf, 1997; Jackson, 2002). We suppose further that the rates of cell birth and death (and, hence, domain growth) are regulated by two diffusible chemical species (these may represent, for example, naturally occurring and cell-derived growth factors, externally supplied species such as oxygen or, perhaps, a cytotoxic drug). For simplicity we assume that tissue growth is one-dimensional and restrict attention to one-dimensional cartesian geometry.

We denote time by t and position in our one-dimensional growing domain by $x \in (-R(t), R(t))$, $R(t)$ representing the domain size at time t. We introduce $\omega(x, t)$ and $V(x, t)$ to represent the local cell density and velocity, respectively. We also use $u(x, t)$ and $v(x, t)$ to represent the concentrations of the two chemicals of interest.

When considering the evolution of the cells we assume that they move by a combination of random motion and advection and we denote by $\tilde{F}(u, v, \omega)$ their net rate of cell proliferation. Using the principle of mass balance, we combine these mechanisms and, in this way, deduce that the evolution of the cell density satisfies

$$\frac{\partial \omega}{\partial t} + \frac{\partial}{\partial x}(\omega V) = \mu \frac{\partial^2 \omega}{\partial x^2} + \tilde{F}(u, v, \omega). \tag{1}$$

In Eq. (1) μ represents the cells' random motility coefficient which we assume to be constant and the net rate of cell proliferation $\tilde{F}$ is defined below.

As for the cell density, we suppose that the evolution of the chemical species is governed by reaction-diffusion-advection so that

$$\frac{\partial u}{\partial t} + \frac{\partial}{\partial x}(uV) = D_u \frac{\partial^2 u}{\partial x^2} + \tilde{f}(u, v, \omega), \tag{2}$$

$$\frac{\partial v}{\partial t} + \frac{\partial}{\partial x}(vV) = D_v \frac{\partial^2 v}{\partial x^2} + \tilde{g}(u, v, \omega). \tag{3}$$

In Eqs. (2) and (3), the positive constants D_u and D_v represent the chemicals' diffusion coefficients while $\tilde{f}$ and $\tilde{g}$ represent their net reaction rates. In practice, our choice of $\tilde{f}$ and $\tilde{g}$ should be motivated by particular cells or biological tissues and specific chemicals. As a specific example, we suppose that u and v undergo Schnakenberg kinetics (1979) so that, in terms of positive rate constants k_1, k_2, k_3 and k_4 we have

$$\frac{\partial u}{\partial t} + \frac{\partial}{\partial x}(uV) = D_u \frac{\partial^2 u}{\partial x^2} + k_1 - k_2 uv, \tag{4}$$

$$\frac{\partial v}{\partial t} + \frac{\partial}{\partial x}(vV) = D_v \frac{\partial^2 v}{\partial x^2} + k_3 - k_4 v + k_2 uv. \tag{5}$$

We note that other kinetic terms such as the well-studied Gierer and Meinhardt (1972) or Gray and Scott (1983) kinetics could also be used: we choose Schnakenberg kinetics to facilitate comparison with related work by Crampin et al. (1999).

We account for domain growth by assuming that the tissue boundary $x = R(t)$ moves with the local cell velocity there. Referring to Eq. (1) we have that the domain size changes in the following manner

$$\frac{\mathrm{d}R}{\mathrm{d}t} = V - \frac{\mu}{\omega}\left.\frac{\partial \omega}{\partial x}\right|_{x=R(t)}. \tag{6}$$

In practice constitutive laws that depend on the mechanical properties of the tissue in question (such as whether it is visco-elastic or elastic) should be used to determine the velocity field $V(x,t)$. Here we exploit the one-dimensional geometry and, following Ward and King (1997) make the constitutive assumption that the tissue maintains a constant cell density, $\omega = \omega^*$ say, as it develops. We note that the cells which undergo cell death have been implicitly, and immediately, removed in the model. This is for simplicity and to keep the link with the work of Crampin et al. (1999) as clear as possible. In practice, it is straightforward to introduce a population of dead cells (for example, see Ward and King, 1999). With $\omega = \omega^*$, Eqs. (1) and (4)–(6) become

$$\frac{\partial u}{\partial t} + \frac{\partial}{\partial x}(uV) = D_u \frac{\partial^2 u}{\partial x^2} + k_1 - k_2 u v, \tag{7}$$

$$\frac{\partial v}{\partial t} + \frac{\partial}{\partial x}(vV) = D_v \frac{\partial^2 v}{\partial x^2} + k_3 - k_4 v + k_2 u v, \tag{8}$$

$$\frac{\partial V}{\partial x} = \frac{1}{\omega^*}\tilde{F}(u, v, \omega^*) \equiv F^*(u, v) \tag{9}$$

with

$$\frac{\mathrm{d}R}{\mathrm{d}t} = V(R, t). \tag{10}$$

We note that for more general (e.g. two-dimensional) geometries specifying $\omega = \omega^*$ would be insufficient to close the model and other, more complex constitutive assumptions are needed. Details of possible closures are discussed in Franks and King (2003).

We now consider the boundary and initial conditions. By assuming symmetry about $x = 0$ we restrict attention to $0 \leq x \leq R(t)$ and impose

$$V = \frac{\partial u}{\partial x} = \frac{\partial v}{\partial x} = 0 \quad \text{at} \quad x = 0. \tag{11}$$

We suppose further that the domain is isolated, with no flux of either chemical across $x = R(t)$, so that

$$\frac{\partial u}{\partial x} = \frac{\partial v}{\partial x} = 0 \quad \text{at} \quad x = R(t). \tag{12}$$

Finally we prescribe initial profiles for u and v and the initial domain size:

$$u(x,0) = u_{\text{in}}(x), \quad v(x,0) = v_{\text{in}}(x), \quad R(0) = R_{\text{in}}. \tag{13}$$

For completeness and to reduce the number of model parameters, we nondimensionalise Eqs. (7)–(13), taking the half-life of v as a typical timescale and the distance over which u diffuses during this period as a typical lengthscale. Accordingly, we rescale the independent and dependent variables by setting

$$x = L\tilde{x}, \quad t = T\tilde{t}, \quad u = \sqrt{\frac{k_4}{k_2}}\tilde{u}, \quad v = \sqrt{\frac{k_4}{k_2}}\tilde{v},$$

$$V = \frac{D_u}{L}\tilde{V} \quad \text{and} \quad R = L\tilde{R}. \tag{14}$$

where

$$T = \frac{1}{k_4} \quad \text{and} \quad L = \sqrt{\frac{D_u}{k_4}}$$

and tildes denote dimensionless variables. Using (14) to rewrite Eqs. (7)–(13) in terms of the dimensionless variables gives (upon dropping the tildes)

$$\frac{\partial u}{\partial t} + \frac{\partial}{\partial x}(Vu) = \frac{\partial^2 u}{\partial x^2} + p - uv^2, \tag{15}$$

$$\frac{\partial v}{\partial t} + \frac{\partial}{\partial x}(Vv) = d\frac{\partial^2 v}{\partial x^2} + q - v + uv^2, \tag{16}$$

$$\frac{\partial V}{\partial x} = F(u,v), \tag{17}$$

$$\frac{\mathrm{d}R}{\mathrm{d}t} = V(R,t), \tag{18}$$

with

$$\frac{\partial u}{\partial x} = 0 = \frac{\partial v}{\partial x} \quad \text{at} \quad x = 0, R(t) \qquad \text{and} \quad V = 0 \quad \text{at} \quad x = 0, \tag{19}$$

$$u = u_{\text{in}}(x), \quad v = v_{\text{in}}(x), \quad \text{and} \quad R = R_{\text{in}} \quad \text{at } t = 0, \tag{20}$$

where

$$p = \frac{k_1}{k_4}\sqrt{\frac{k_2}{k_4}}, \quad q = \frac{k_3}{k_4}\sqrt{\frac{k_2}{k_4}}, \quad F(u,v) = \frac{1}{k_4}F^*(u,v) \quad \text{and} \quad d = \frac{D_v}{D_u}.$$

Equations (15)–(20) constitute our one-dimensional model for tissue growth when this growth is intimately related to the behaviour of chemicals that react and diffuse within the domain.

3. Numerical simulations

In this section we use numerical methods to investigate the impact that domain growth has on the spatial patterns that emerge (and vice versa) for two simple choices of the local cell proliferation rate, $F(u, v)$. In Section 3.2 we prescribe $F(u, v) = \rho$, constant and explain how this case corresponds to exponential domain growth as studied by Crampin et al. (1999). When $F(u, v) = \rho$, domain growth is independent of the diffusible chemicals and we concentrate on showing how domain growth influences the structure of the emerging patterns. In Section 3.3 we fix $F(u, v) = \alpha u - \beta v$ for constants α and β so that the evolution of the domain size is coupled to that of the chemicals. Before presenting our findings for the two choices of $F(u, v)$, we outline the numerical method used to solve the model equations.

3.1. Numerical method

In order to construct numerical solutions to our model equations it is convenient first to map the problem onto a fixed domain $0 \le \xi \le 1$ (Crank, 1984) such that

$$(x, t) \longrightarrow (\xi, \tau) = \left(\frac{x}{R(t)}, t\right). \tag{21}$$

Under this mapping Eqs. (15)–(20) transform to give (substituting $t = \tau$)

$$\frac{\partial u}{\partial t} + \frac{1}{R}\left(V - \xi\frac{\mathrm{d}R}{\mathrm{d}t}\right)\frac{\partial u}{\partial \xi} = \frac{1}{R^2(t)}\frac{\partial^2 u}{\partial \xi^2} + p - uv^2 - uF(u, v), \tag{22}$$

$$\frac{\partial v}{\partial t} + \frac{1}{R}\left(V - \xi\frac{\mathrm{d}R}{\mathrm{d}t}\right)\frac{\partial v}{\partial \xi} = \frac{d}{R^2(t)}\frac{\partial^2 v}{\partial \xi^2} + q - v + uv^2 - vF(u, v), \tag{23}$$

$$\frac{1}{R}\frac{\partial V}{\partial \xi} = F(u, v), \tag{24}$$

$$\frac{\mathrm{d}R}{\mathrm{d}t} = V(1, t), \tag{25}$$

with

$$\frac{\partial u}{\partial \xi} = 0 = \frac{\partial v}{\partial \xi} \quad \text{at} \quad \xi = 0, 1, \tag{26}$$

$$V = 0 \quad \text{at} \quad \xi = 0, \tag{27}$$

$$u = u_{\text{in}}(\xi), \quad v = v_{\text{in}}(\xi) \quad \text{and} \quad R = R_{\text{in}} \quad \text{at} \quad t = 0. \tag{28}$$

We use the NAG routine D03PCF to solve Eqs. (22)–(28) and we note that a uniform grid is used throughout (rather than adapting the grid to the increasing domain size). The trapezium rule is used to integrate (24) to solve for the velocity, V. A second numerical code was developed to test the accuracy of the NAG routine method. The alternative approach involved assuming a Fourier decomposition for u and v in terms of cosine series so that boundary conditions (26) and (27) were automatically satisfied and Eq. (24) could be integrated analytically. The two numerical methods agreed closely (results not shown); the results shown here were obtained with the former method.

3.2. *Exponential domain growth*

Fixing $F(u, v) = \rho =$ constant, we integrate Eq. (17) subject to (19) to find

$$V(x, t) = \rho x \tag{29}$$

so that the local cell velocity increases (decreases) linearly with position x if $\rho > 0$ ($\rho < 0$). Using (29) and assuming $R(0) = 1$ in (18) gives

$$R(t) = e^{\rho t}. \tag{30}$$

Hence when $F(u, v) = \rho$ there is exponential domain growth and our model is identical to that presented in Crampin et al. (1999), even though Crampin et al. did not introduce cell velocity explicitly into their model. As a result of our more detailed derivation we are able to predict the type of cellular behaviour that would yield such exponential domain growth. In particular, if the net cell proliferation rate is constant at all points within the domain and, hence, not affected by the local concentration of u or v, then we predict that the tissue will grow exponentially.

We note further that with $V(x, t) = \rho x$ (or, equivalently, $V(\xi, t) = \rho R(t)\xi$) and $R(t) = \exp(\rho t)$ Eqs. (22) and (23), the governing equations for u and v on the fixed domain, simplify to give

$$\frac{\partial u}{\partial t} = \frac{1}{R^2(t)}\frac{\partial^2 u}{\partial \xi^2} + p - uv^2 - \rho u, \tag{31}$$

$$\frac{\partial v}{\partial t} = \frac{d}{R^2(t)}\frac{\partial^2 v}{\partial \xi^2} + q - v + uv^2 - \rho v. \tag{32}$$

The sink terms $-\rho u$ and $-\rho v$ that appear in (31) and (32) represent chemical dilution due to domain expansion (assuming $\rho > 0$). These terms were neglected in Crampin et al. (1999) and, so, a main focus of the numerical results presented below is to identify conditions under which this approximation is valid.

In order to facilitate comparison with Crampin et al. (1999) results, where possible we make the same choice of parameter values. Thus, unless otherwise stated, in Eqs. (31) and (32) we fix

$$d = 0.01, \quad p = 0.9, \quad q = 0.1,$$

leaving the local cell proliferation rate, ρ, as a free parameter. In this case, when $\rho = 0$, the spatially uniform, steady state solution of Eqs. (22) and (23) has coordinates $(u, v) = (u_0, v_0)$ where

$$(u_0, v_0) = \left(\frac{p}{(p+q)^2}, p+q \right) \equiv (0.9, 1.0)$$

and the initial conditions are periodic perturbations about this steady state of the form

$$u_{\text{in}}(\xi) = u_0 + 0.01 \cos(\pi \xi) \quad \text{and} \quad v_{\text{in}}(\xi) = v_0.$$

We note that for ρ nonzero the uniform steady state and its stability may be changed. Indeed, under certain conditions, the likelihood of spatial pattern is increased when dilution effects are included (see Neville, 2003 for details).

In Fig. 1 we present results of the case of weak dilution or slow domain growth ($\rho = 0.01$) that are in good agreement with the simulations presented in Crampin

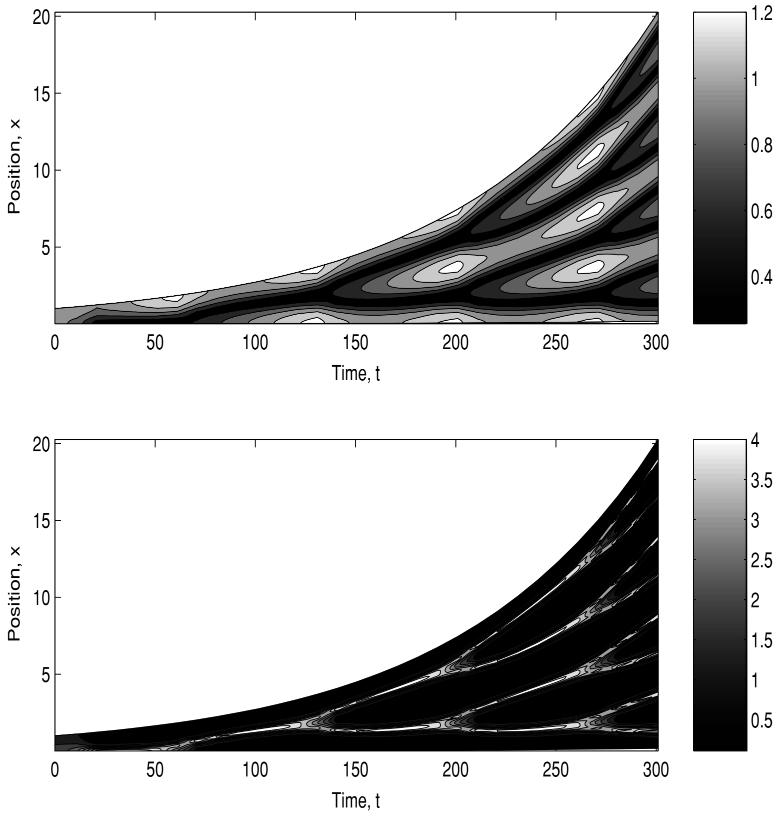

Fig. 1 Simulation results depicting evolution of u (*upper panel*) and v (*lower panel*) concentration profiles for Schnakenberg kinetics on an exponentially growing domain when dilution effects are retained. These profiles are indistinguishable from those without dilution (results not shown). Parameter values: $d = 0.01$, $p = 0.9$, $q = 0.1$ and $\rho = 0.01$.

et al. (1999). In both cases, the activator u and inhibitor v are in spatial antiphase, as would be anticipated for a system such as Schnakenberg that exhibits cross kinetics. Pattern transitions are by peak splitting (generated from initial data close to a uniform steady state) and the spatial frequency of the system regularly doubles. No other pattern modes enter the sequence.

Our simulations show that for $\rho \ll 1$ inclusion of the dilution terms $-u\rho$ and $-v\rho$ in (31) and (32) does not noticeably affect the pattern solutions (see Fig. 1). However, we will now see that for larger values of ρ these terms must be retained if accurate predictions regarding pattern selection are to be made.

Comparing Figs. 2 and 3, we see that when ρ is increased from $\rho = 0.01$ to $\rho = 0.1$ dilution greatly influences the generated pattern. While in both cases frequency-doubling is absent, the distribution of u and v throughout the domain varies greatly according to whether or not dilution is included. When it is included (Fig. 2) peak-splitting arises for certain modes but is absent for others. There seems

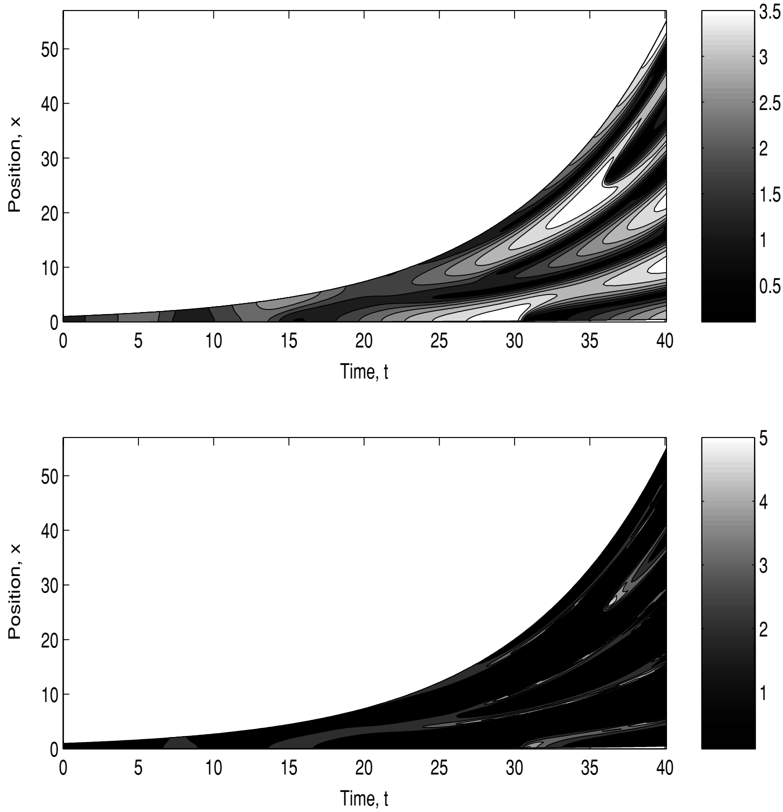

Fig. 2 Simulation results depicting profiles of u (*upper panel*) and v (*lower panel*), when the domain grows exponentially, the chemicals interact via Schnackenberg kinetics and dilution terms are retained. Comparison with Fig. 3 shows that, in this case, retention of dilution effects leads to more marked spatial variation in u and v. Parameter values: $d = 0.01$, $p = 0.9$, $q = 0.1$ and $\rho = 0.1$.

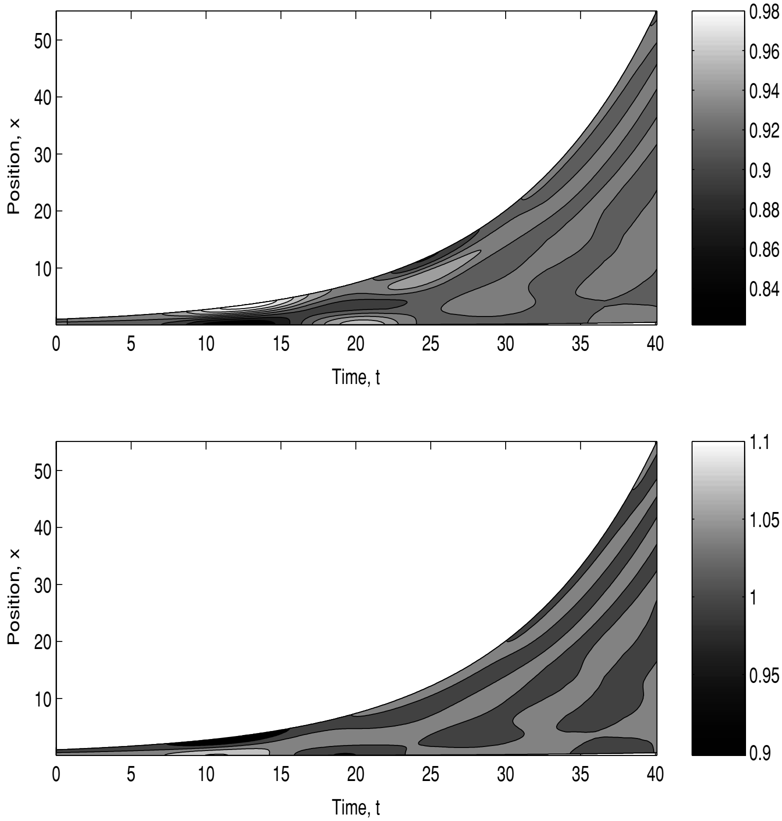

Fig. 3 Simulation results depicting profiles of u (*upper panel*) and v (*lower panel*) when the domain grows exponentially, the chemicals interact via Schnackenberg kinetics and dilution terms are neglected. Parameter values: as per Fig. 2.

to be no regular splitting and the system is spatially and temporally unstable. In Fig. 3 dilution effects are neglected and patterning is suppressed: u and v remain near u_0 and v_0 for all x and t.

Figure 4 shows that the total amount of u present is much higher when dilution is included than when it is neglected. The converse is true for v (results not included). This situation is a direct consequence of the cross kinetics of the Schnakenberg system: u activates the production of v while v inhibits the production of u. When dilution is included the rate at which v stimulates its own production is reduced, so it is less effective at inhibiting the production of u. Also, although u becomes slightly better at self-inhibition its activation of v is lowered. As a result, when dilution is included the total concentration of v within the domain is lowered and the total concentration of u is raised.

We remark that the above results are not peculiar to the Schnakenberg kinetics: similar results were obtained for other choices of the kinetic terms, including

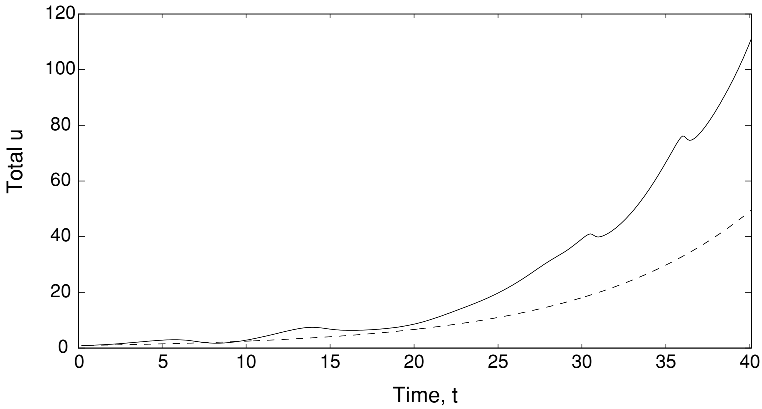

Fig. 4 Diagram showing how $u_{\text{total}}(t) = \int_0^{R(t)} u(x,t)\,\mathrm{d}x$ evolves over time. Key: solid (*dashed*) lines represent model solutions with (without) dilution effects included. Parameter values: as per Fig. 2.

Gierer-Meinhardt kinetics (Gierer and Meinhardt, 1972) (for details see Neville, 2003).

3.3. Non-uniform domain growth

In the previous section, we focused on exponential domain growth, a situation that arises when the net cell proliferation rate is independent of u and v. In practice cell division and death may be strongly influenced by chemicals present within their environment (Jones et al., 2000; Murray and Hunt, 1993; Santini et al., 2000). For these reasons it may be more appropriate to suppose that the net cell birth rate (and hence the net rate of domain growth) depends on the chemicals u and v. While in general, the proliferation rate $F(u, v)$ may be a nonlinear function, for simplicity we choose a simple linear form. Accordingly we introduce non-negative constants α and β such that in Eq. (17)

$$F(u, v) = \alpha u - \beta v. \tag{33}$$

In using (33), we are assuming that u promotes cell growth (like oxygen or glucose) and that v inhibits growth (like a cytotoxic drug). Provided that u and v are not spatially uniform, this will give rise to nonuniform cell growth. We present below numerical solutions of Eqs. (15)–(20) with $F(u, v)$ specified by Eq. (33).

Repeated simulations indicate that the behaviour of the system is strongly influenced by the choice of parameter values. In particular the domain does not always grow: its size may remain unchanged or shrink (see Figs. 5 and 6). Figure 5 shows spatially uniform chemical distributions which increase in magnitude over time, whereas in Fig. 6 the spatial perturbations decay rapidly, leaving profiles that are spatially uniform steady states. This occurs because, for the parameter values used

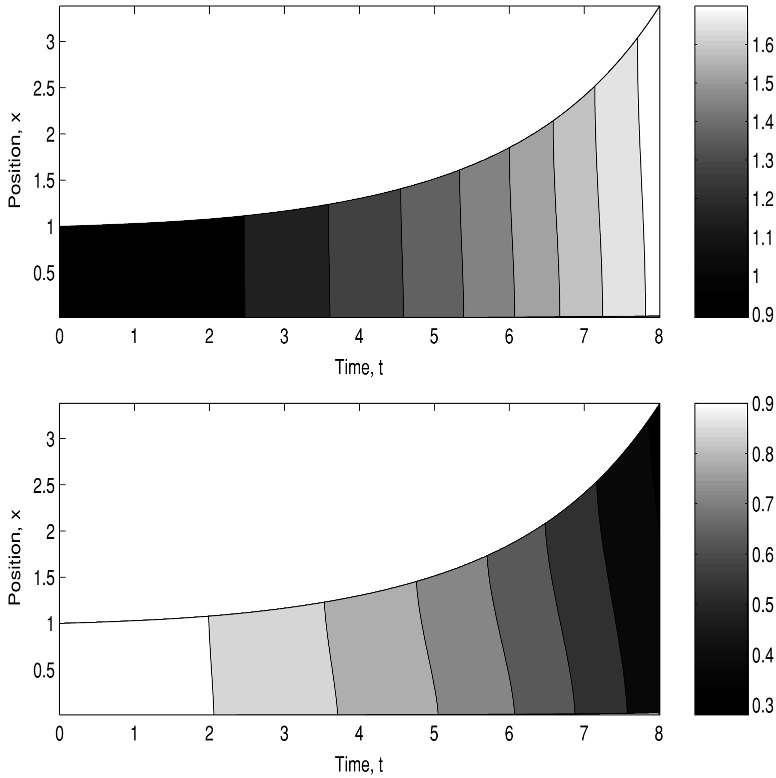

Fig. 5 Simulation results depicting u (*upper panel*) and v (*lower panel*) when $F(u, v) = \alpha u - \beta v$ and the chemicals interact via Schnakenberg kinetics. Domain growth is approximately exponential and, although there is no spatial patterning, the levels of u (and v) increase (and decrease) over time. Parameter values: $d = 0.01$, $p = 0.9$, $q = 0.1$, $\alpha = 0.25$ and $\beta = 0.20$. Initial conditions: $u = u_0 + 0.01 \cos(\pi x)$, $v = v_0$ and $R = 1$ at $t = 0$.

to construct Fig. 6, the uniform steady state of Eqs. (15)–(18) is stable (the analysis presented in Section 4.1 can be used to confirm this).

If the system is initially perturbed from a stable steady state we might expect the sign of $\alpha u_0 - \beta v_0$ to influence the domain growth rate, with expansion occurring if $\alpha u_0 - \beta v_0 > 0$ and regression if $\alpha u_0 - \beta v_0 < 0$. While the simulations are consistent with this claim, when $\alpha_0 u_0 = \beta v_0$ the domain size does not necessarily remain fixed, due to the perturbations in u and v which force $\alpha u - \beta v \neq 0$. This may lead to expansion or shrinkage of the domain (see Fig. 7). We note also that if the domain size is too small then no patterns are discernible (see Fig. 8).

In general, the numerical results show a complicated interaction between the chemical patterns and the domain size. As the patterns grow, $\alpha u - \beta v$ changes so the rate of domain growth changes. Conversely, as the domain size changes, the growth rate of the spatial patterns is altered, partly by the dilution terms and partly because the allowable wavenumbers of patterns are changing. It is not clear from

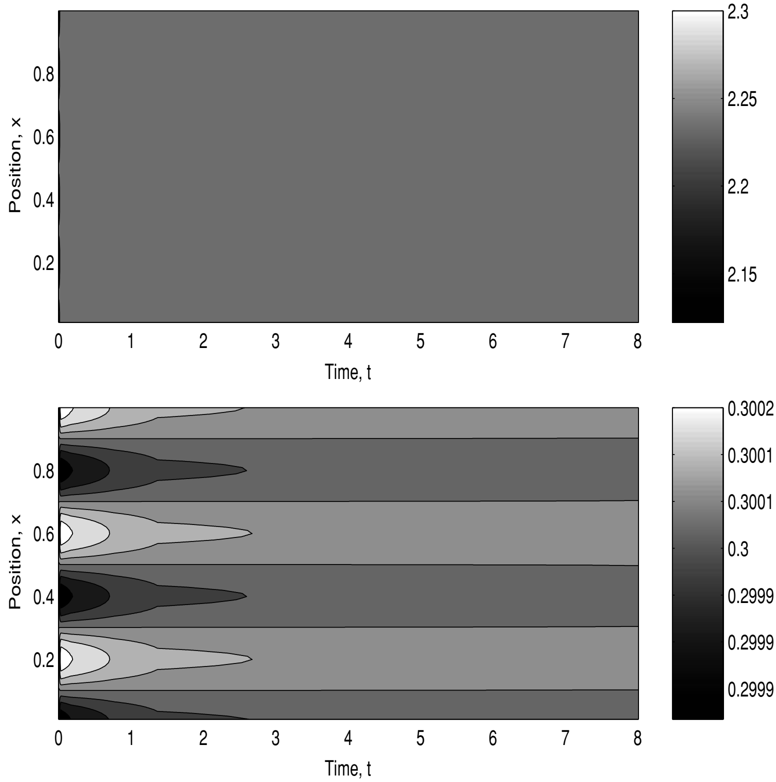

Fig. 6 Simulation results (as filled contour plots) depicting u (*upper panel*) and v (*lower panel*) when $F(u, v) = \alpha u - \beta v$ and the chemicals interact via Schnakenberg kinetics. In this case $\alpha u_0 = \beta v_0$ and the system settles rapidly to an equilibrium with no domain growth and minimal spatial variation in u and v. Parameter values: $d = 0.01$, $p = 0.2$, $q = 0.1$, $\alpha = 0.30$ and $\beta = 2.2$. Initial conditions: $u = u_0 + 0.1 \cos(5\pi x)$, $v = v_0$ and $R = 1$ at $t = 0$.

the simulations whether the predominant effect is the domain size regulating the chemical patterns or vice versa. As the analysis of Section 4 demonstrates, the two effects are linked in a complex nonlinear manner.

4. Weakly nonlinear analysis

In this section, we construct approximate solutions for a generalised version of our model of pattern formation on a growing domain, assuming that the patterns are small perturbations from the spatially uniform state. This analysis provides insight into some aspects of the interactions between the diffusible chemicals and the evolving domain reported in Section 3. We note that the timescale of interest here is distinct from other weakly nonlinear analyses such as Benson et al. (1998), Byrne and Matthews (2002) and Matthews (1998).

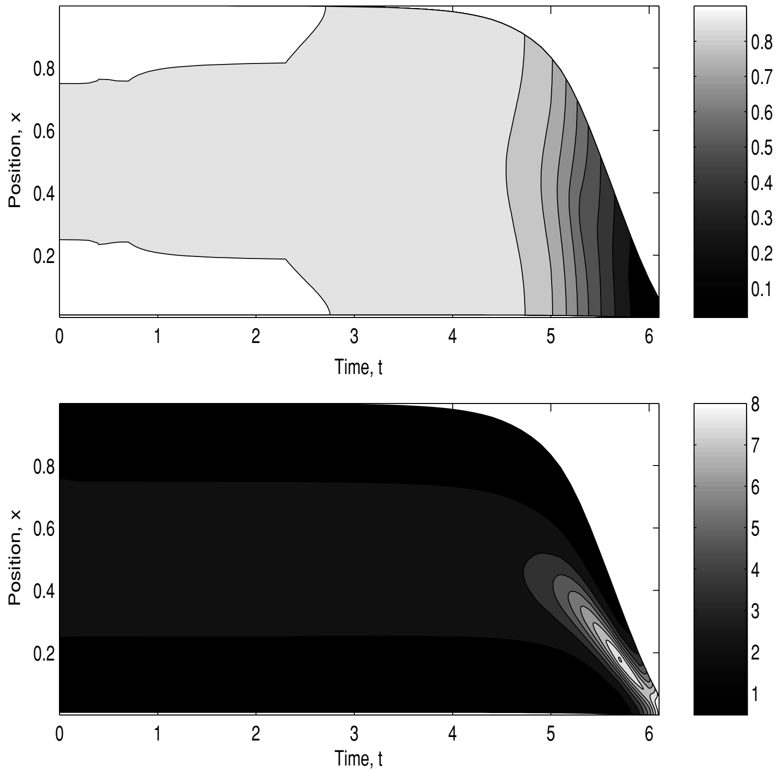

Fig. 7 Simulation results depicting u (*upper panel*) and v (*lower panel*) when $F(u, v) = \alpha u - \beta v$ and the chemicals interact via Schnakenberg kinetics. As in Fig. 6, $\alpha u_0 = \beta v_0$. However, in this case, following a long period ($0 < t < 2.5$) during which the spatial pattern remains stable and the domain boundary remains constant ($R \equiv 1$), the domain starts to decrease in size. This behaviour persists until the domain size falls below a threshold size at which time ($t \sim 3$) the u component ceases to vary and the v component has only small spatial variations. Thereafter the domain rapidly shrinks and spatial patterns in both u and v emerge. Parameter values: $d = 0.01$, $p = 0.9$, $q = 0.1$, $\alpha = 1.00$ and $\beta = 0.90$. Initial conditions: $u = u_0 + 0.01\cos(2\pi x)$, $v = v_0$ and $R = 1$ at $t = 0$.

Replacing the Schnakenberg kinetics of Sections 2 and 3 by general kinetic terms $f(u, v)$ and $g(u, v)$ and denoting by $F(u, v)$ the local cell proliferation rate, we now study the following, generalised version of Eqs. (15)–(20):

$$\epsilon \frac{\partial u}{\partial \tau} + \frac{\partial}{\partial x}(Vu) = \frac{\partial^2 u}{\partial x^2} + f(u, v), \tag{34}$$

$$\epsilon \frac{\partial v}{\partial \tau} + \frac{\partial}{\partial x}(Vv) = d\frac{\partial^2 v}{\partial x^2} + g(u, v), \tag{35}$$

$$\frac{\partial V}{\partial x} = F(u, v), \tag{36}$$

$$\epsilon \frac{\mathrm{d}R}{\mathrm{d}\tau} = V(R, \tau), \tag{37}$$

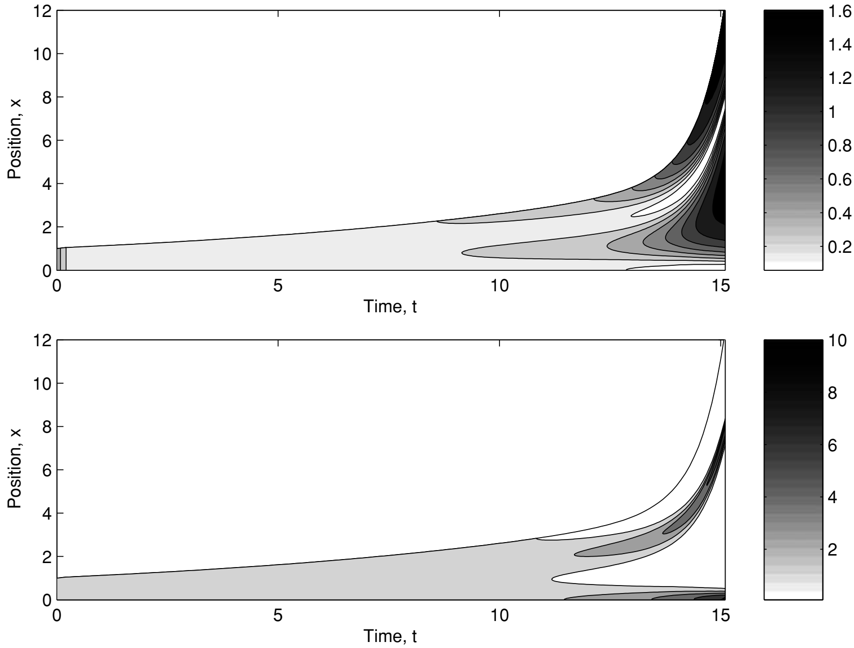

Fig. 8 Simulation results depicting u (*upper panel*) and v (*lower panel*) when $F(u, v) = \alpha u - \beta v$ and the chemicals interact via Schnakenberg kinetics. In this case the equilibrium values are $(u_0, v_0) = (0.3122, 3.1)$ so that $\alpha u_0 - \beta v_0 = 0.0022$. Following a long period $(0 < t < 9)$ of slow domain growth during which the concentrations of u and v remain approximately constant the domain size increases through the threshold value for which spatial patterning may occur. Thereafter (for $t \geq 12$) domain growth increases rapidly and the chemicals develop spatial patterns. Parameter values: $d = 0.01$, $p = 3.0$, $q = 0.1$, $\alpha = 1.00$ and $\beta = 0.10$. Initial conditions: $u = 0.73$, $v = 2.83$ and $R(t) = 1$ at $t = 0$.

with

$$\frac{\partial u}{\partial x} = 0 = \frac{\partial v}{\partial x} \quad \text{at} \quad x = 0, R(\tau) \qquad \text{and} \quad V = 0 \quad \text{at} \quad x = 0, \tag{38}$$

$$u = u_{\text{in}}(x), \quad v = v_{\text{in}}(x), \quad R = R_{\text{in}} \quad \text{at} \quad \tau = 0. \tag{39}$$

In (39) the functions $u_{\text{in}}(x)$, $v_{\text{in}}(x)$ and the initial tumour radius R_{in} are assumed to be compatible with the trial solutions sought below.

In Eqs. (34)–(39), we have introduced a small parameter $0 < \epsilon \ll 1$ to characterise the amplitude of the pattern forming perturbations in u and v and assumed that the timescale of interest is long so that $\tau = \epsilon t$. We remark that this renders our analysis distinct from similar weakly nonlinear analyses of pattern formation on fixed domains where the relevant timescale $\epsilon^2 t$ is longer (see, for example, Grindrod, 1996 page 82).

We construct trial solutions, which are perturbations about the spatially uniform steady state so that

$$u(x,\tau) = u_0 + \epsilon u_1(x,\tau) + \epsilon^2 u_2(x,\tau) + O(\epsilon^3), \tag{40}$$

$$v(x,\tau) = v_0 + \epsilon v_1(x,\tau) + \epsilon^2 v_2(x,\tau) + O(\epsilon^3), \tag{41}$$

$$V(x,\tau) = \epsilon V_1(x,\tau) + \epsilon^2 V_2(x,\tau) + O(\epsilon^3), \tag{42}$$

$$R(\tau) = R_0 + \epsilon R_1(\tau) + \epsilon^2 R_2(\tau) + O(\epsilon^3), \tag{43}$$

where the constants u_0 and v_0 satisfy

$$0 = f(u_0, v_0) = g(u_0, v_0) = F(u_0, v_0) \tag{44}$$

in order that the governing equations hold at leading order. Thus in the spatially uniform state there is no domain growth. In general, Eq. (44) overspecifies u_0 and v_0: for given choices of f, g and F, the third equation yields a relationship between the system parameters that must be satisfied to realise solutions of this type. For example, with Schnakenberg kinetics and $F(u, v) = \alpha u - \beta v$, we have

$$u_0 = \frac{p}{(p+q)^2} \quad \text{and} \quad v_0 = p + q$$

and we require

$$\frac{\alpha}{\beta} = \frac{v_0}{u_0} \equiv \frac{(p+q)^3}{p}.$$

In the case of α or β equal to zero, our analysis breaks down and so (33) would need modifying. We note also that the leading order tumour radius R_0 remains unspecified: we show below how it is determined at $O(\epsilon)$.

4.1. $O(\epsilon)$ analysis

Continuing to $O(\epsilon)$, we deduce that u_1 and v_1 solve

$$0 = \frac{\partial^2 u_1}{\partial x^2} + (f_u - u_0 F_u)u_1 + (f_v - u_0 F_v)v_1, \tag{45}$$

$$0 = d\frac{\partial^2 v_1}{\partial x^2} + (g_u - v_0 F_u)u_1 + (g_v - v_0 F_v)v_1, \tag{46}$$

where subscripts u and v denote partial derivatives with respect to u and v evaluated at $(u, v) = (u_0, v_0)$. We may write (45) and (46) more succinctly as

$$\mathcal{L}\boldsymbol{u_1} = 0 \tag{47}$$

where $\boldsymbol{u_1} = (u_1, v_1)$ and $\mathcal{L}$ is a second order differential operator. When deriving Eqs. (45) and (46) we have eliminated V_1 which satisfies

$$\frac{\partial V_1}{\partial x} = F_u u_1 + F_v v_1, \quad \text{with} \quad V_1 = 0 \quad \text{at} \quad x = 0. \tag{48}$$

Equations (45) and (46) are closed by applying the following boundary conditions:

$$0 = \frac{\partial u_1}{\partial x} = \frac{\partial v_1}{\partial x} \quad \text{at} \quad x = 0,\ R_0. \tag{49}$$

We assume that separable solutions exist in the form

$$(u_1, v_1) = A(\tau)(\mu_1, \nu_1)\cos kx \tag{50}$$

where the amplitude $A(\tau)$ is determined at higher order and the constants μ_1, ν_1 and the spatial wavenumber k are determined at $O(\epsilon)$. For example, Eqs. (45) and (46) yield

$$\nu_1 = -\frac{(-k^2 + f_u - F_u u_0)}{f_v - F_v u_0}\,\mu_1,$$

together with the following condition for k:

$$0 = dk^4 - \left\{(g_v - F_v v_0) + d(f_u - F_u u_0)\right\}k^2 + \Delta, \tag{51}$$

where

$$\Delta = (f_u - u_0 F_u)(g_v - v_0 F_v) - (f_v - u_0 F_v)(g_u - v_0 F_u).$$

Additionally, imposing the no-flux boundary conditions at $x = R_0$ we deduce that R_0 satisfies

$$R_0 = \frac{n\pi}{k}, \quad n = 0, 1, 2, 3, \ldots. \tag{52}$$

We note also that, with $\boldsymbol{u}_1$ specified by (50), the velocity profile is given by

$$V_1 = \frac{A(\tau)}{k}\,(F_u\mu_1 + F_v\nu_1)\sin kx. \tag{53}$$

The above expressions indicate how the coupling between the domain growth rate and the kinetics of the chemicals becomes manifest. For example, the appearance of terms of the form F_u and F_v in Eq. (51) shows clearly how domain growth affects the critical value of d as a function of wavenumber k at which spatial patterns may emerge. Equally, with k defined in terms of model parameters by (51), Eq. (52) shows how the domain size at which patterns emerge depends on the chemical kinetics and the domain growth rate itself. At this order, (53) shows that there is local expansion and contraction, but the net effect of this cancels out, leading to zero velocity on the boundary and so no net growth of the domain.

In the case $F(u, v) = \alpha u - \beta v$, with $\beta = \alpha u_0/v_0$ to satisfy (44), the dispersion relation (51) for the Schnakenberg system becomes

$$\begin{aligned} &dk^4 + (\alpha u_0(d-1) + dv_0^2 + 1 - 2u_0v_0)k^2 \\ &\quad + v_0^2 - 3u_0v_0\alpha(u_0+v_0) + \alpha u_0 = 0. \end{aligned} \tag{54}$$

This can be solved to give the critical value for d at the onset of pattern formation, as a function of wavenumber k.

$$d(k) = \frac{k^2(\alpha u_0 - 1 + 2u_0v_0) - v_0^2 + 3u_0v_0\alpha(u_0+v_0) - \alpha u_0}{k^4 + k^2(\alpha u_0 + v_0^2)}. \tag{55}$$

Thus, although there is no net growth at this order, the linear stability condition for the onset of pattern formation is modified by the inclusion of chemical-dependent growth. It can be shown by differentiating $d(k)$ with respect to α that $d(k)$ increases with α. This means that the inclusion of the chemical-dependent growth makes the system more unstable to pattern formation (recall that we are assuming $\alpha > 0$). Figure 9 shows a plot of $d(k)$ for three values of α.

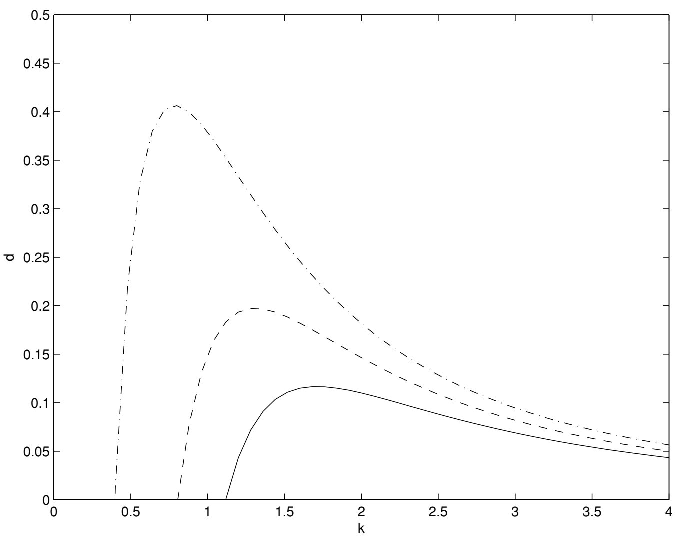

Fig. 9 Series of linear stability curves for the Schnakenberg model for three choices of α. The curves show how the critical value of d at the onset of pattern formation varies with the spatial wavenumber k (see Eq. (55)). As α increases the size of the region below the critical curve in (d, k) parameter space in which the uniform steady state is linearly unstable also increases. Parameter values: $p = 0.9$, $q = 0.1$ and $\alpha = 0$ (*solid line*), $\alpha = 0.1$ (*dashed line*), $\alpha = 0.2$ (*dash-dot line*).

4.2. $O(\epsilon^2)$ analysis—$O(\epsilon)$ amplitude variation

We now extend our analysis to $O(\epsilon^2)$ in order to determine how the amplitude $A(\tau)$ and the domain size evolve over time. Equating to zero coefficients of $O(\epsilon^2)$ it is straightforward to show that $\boldsymbol{u_2} = (u_2, v_2)$ and R_1 solve

$$\mathcal{L}\boldsymbol{u_2} = \mathcal{F}(\boldsymbol{u_1}), \tag{56}$$

$$\frac{\mathrm{d}R_1}{\mathrm{d}\tau} = V_2(R_0, \tau) + R_1 \frac{\partial V_1}{\partial x}(R_0, \tau), \tag{57}$$

where $\mathcal{L}$ was defined at $O(\epsilon)$ (see Eqs. (45)–(47)),

$$\mathcal{F}(\boldsymbol{u_1}) = \begin{cases} \dfrac{\partial u_1}{\partial \tau} + \dfrac{\partial}{\partial x}(u_1 V_1) - \dfrac{1}{2}(f_{uu}u_1^2 + 2f_{uv}u_1v_1 + f_{vv}v_1^2) \\ \qquad\qquad + \dfrac{u_0}{2}(F_{uu}u_1^2 + 2F_{uv}u_1v_1 + F_{vv}v_1^2) \\ \\ \dfrac{\partial v_1}{\partial \tau} + \dfrac{\partial}{\partial x}(v_1 V_1) - \dfrac{1}{2}(g_{uu}u_1^2 + 2g_{uv}u_1v_1 + g_{vv}v_1^2) \\ \qquad\qquad + \dfrac{v_0}{2}(F_{uu}u_1^2 + 2F_{uv}u_1v_1 + F_{vv}v_1^2) \end{cases}$$

and

$$\frac{\partial V_2}{\partial x} = F_u u_2 + F_v v_2 + \frac{1}{2}(F_{uu}u_1^2 + 2F_{uv}u_1v_1 + F_{vv}v_1^2). \tag{58}$$

Equations (56) and (57) are closed by imposing the following boundary and initial conditions

$$0 = \frac{\partial u_2}{\partial x} = \frac{\partial v_2}{\partial x} = V_2 \quad \text{at} \quad x = 0, \tag{59}$$

$$\frac{\partial u_2}{\partial x} + R_1\frac{\partial^2 u_1}{\partial x^2} = 0 = \frac{\partial v_2}{\partial x} + R_1\frac{\partial^2 v_1}{\partial x^2} \quad \text{at} \quad x = R_0, \tag{60}$$

$$R_1(0) = 0. \tag{61}$$

We do not need to solve the second order problem in order to find the evolution equations for $A(\tau)$ and $R_1(\tau)$. Only certain integrals of the second order variables are required, so we define

$$\mathcal{M}_{20} = \int_0^{R_0} u_2 \mathrm{d}x \quad \text{and} \quad \mathcal{N}_{20} = \int_0^{R_0} v_2 \mathrm{d}x,$$

$$\mathcal{M}_{21} = \int_0^{R_0} u_2 \cos kx \mathrm{d}x \quad \text{and} \quad \mathcal{N}_{21} = \int_0^{R_0} v_2 \cos kx \mathrm{d}x.$$

The following pairs of equations for $(\mathcal{M}_{20}, \mathcal{N}_{20})$ and $(\mathcal{M}_{21}, \mathcal{N}_{21})$ may be obtained by premultiplying Eq. (56) by the relevant factors and integrating with respect to x:

$$(f_u - u_0 F_u)\mathcal{M}_{20} + (f_v - u_0 F_v)\mathcal{N}_{20} = \theta_2 R_0 A^2 - \mu_1 k^2 A R_1 \cos(k R_0) \tag{62}$$

$$(g_u - v_0 F_u)\mathcal{M}_{20} + (g_v - v_0 F_v)\mathcal{N}_{20} = \gamma_2 R_0 A^2 - d\nu_1 k^2 A R_1 \cos(k R_0) \tag{63}$$

and

$$(-k^2 + f_u - u_0 F_u)\mathcal{M}_{21} + (f_v - u_0 F_v)\mathcal{N}_{21} = \mu_1 \left(\frac{R_0}{2} \frac{\mathrm{d}A}{\mathrm{d}\tau} - k^2 R_1 A \right) \tag{64}$$

$$(g_u - v_0 F_u)\mathcal{M}_{21} + (-dk^2 + g_v - v_0 F_v)\mathcal{N}_{21} = \nu_1 \left(\frac{R_0}{2} \frac{\mathrm{d}A}{\mathrm{d}\tau} - dk^2 R_1 A \right) \tag{65}$$

where

$$\theta_2 = \frac{u_0}{4}(F_{uu}\mu_1^2 + 2F_{uv}\mu_1\nu_1 + F_{vv}\nu_1^2) - \frac{1}{4}(f_{uu}\mu_1^2 + 2 f_{uv}\mu_1\nu_1 + f_{vv}\nu_1^2),$$

$$\gamma_2 = \frac{v_0}{4}(F_{uu}\mu_1^2 + 2F_{uv}\mu_1\nu_1 + F_{vv}\nu_1^2) - \frac{1}{4}(g_{uu}\mu_1^2 + 2g_{uv}\mu_1\nu_1 + g_{vv}\nu_1^2).$$

Using the $O(\epsilon)$ condition (51) in Eqs. (64) and (65) we deduce that, for a nontrivial solution, the amplitude $A(\tau)$ must satisfy

$$\frac{\mathrm{d}A}{\mathrm{d}\tau} = \frac{2k^2 A R_1}{R_0} \left(\frac{1 + d\Lambda}{1 + \Lambda} \right) \quad \text{where} \quad \Lambda = \frac{(-k^2 + f_u - u_0 F_u)}{(-dk^2 + g_v - v_0 F_v)}. \tag{66}$$

It remains to determine how R_1 evolves over time. We note from Eqs. (57) and (58) that

$$\begin{aligned} \frac{\mathrm{d}R_1}{\mathrm{d}\tau} &= (F_u \mathcal{M}_{20} + F_v \mathcal{N}_{20}) + \frac{R_0}{4}(F_{uu}\mu_1^2 + 2F_{uv}\mu_1\nu_1 + F_{vv}\nu_1^2)A^2 \\ &\quad + (F_u\mu_1 + F_v\nu_1) A R_1 \cos k R_0. \end{aligned} \tag{67}$$

In Eq. (67), $(\mathcal{M}_{20}, \mathcal{N}_{20})$ satisfy (62) and (63), with solution

$$\begin{pmatrix} \mathcal{M}_{20} \\ \mathcal{N}_{20} \end{pmatrix} = \begin{pmatrix} a_m \\ a_n \end{pmatrix} R_0 A^2 + \begin{pmatrix} b_m \\ b_n \end{pmatrix} k^2 A R_1 \cos k R_0$$

where

$$\begin{pmatrix} a_m \\ a_n \end{pmatrix} = \frac{1}{\Delta} \begin{pmatrix} (g_v - v_0 F_v) & -(f_v - u_0 F_v) \\ -(g_u - v_0 F_u) & (f_u - u_0 F_u) \end{pmatrix} \begin{pmatrix} \theta_2 \\ \gamma_2 \end{pmatrix}$$

and

$$\begin{pmatrix} b_m \\ b_n \end{pmatrix} = -\frac{1}{\Delta} \begin{pmatrix} (g_v - v_0 F_v) & -(f_v - u_0 F_v) \\ -(g_u - v_0 F_u) & (f_u - u_0 F_u) \end{pmatrix} \begin{pmatrix} \mu_1 \\ d\nu_1 \end{pmatrix}.$$

After some algebra, it is possible to show that the coefficient of AR_1 in (67) vanishes and, hence, that the evolution of R_1 is given by

$$\frac{\mathrm{d}R_1}{\mathrm{d}\tau} = R_0 A^2 \left(\frac{1}{4}[F_{uu}\mu_1^2 + 2F_{uv}\mu_1\nu_1 + F_{vv}\nu_1^2] + [F_u a_m + F_v a_n] \right). \tag{68}$$

Equations (66) and (68) show how the slow $O(\epsilon)$ amplitude variation (A) of the spatial patterns (see Eq. (50)) and the $O(\epsilon)$ correction to the domain size R_1 evolve over time. The properties of these equations are investigated in the following section.

4.3. Behaviour of the amplitude equations

Equations (66) and (68) can be written in the following form:

$$\frac{\mathrm{d}A}{\mathrm{d}\tau} = QAR_1, \tag{69}$$

$$\frac{\mathrm{d}R_1}{\mathrm{d}\tau} = PA^2, \tag{70}$$

where P and Q are constants that in general may be positive or negative. It is clear from (66) and (68) that in general, P and Q are finite and non-zero.

Equation (69) states that the growth rate of the pattern is proportional to the perturbation R_1 of the domain size from R_0. Recall that R_0 is defined by the condition (52) which arises from specifying that the linear growth rate is zero at leading order. In general, it is to be expected that the pattern growth rate will be linear in R_1, since as R varies, so does k and the growth rate. (Exceptionally, if d corresponds to a maximum in Fig. 9, then $Q = 0$ and the first nonzero term in (69) would be of order ϵ^3 and proportional to AR_1^2). This interpretation suggests another way to find the coefficient Q: find the derivative of the linear growth rate with respect to R_0, when the growth rate is zero. We have verified that this gives the same value of Q as given in (66).

In Eq. (70) there is no domain growth at linear order, as already discussed, but the domain grows quadratically with the pattern amplitude A. This is because the linear solutions are proportional to $\cos kx$, with zero mean, but their square has a non-zero mean.

The system (69) and (70) has a symmetry $A \leftrightarrow -A$. Also, there is a line of fixed points along $A = 0$, corresponding to the fact that the uniform basic state exists for all values of R. The Eqs. (69) and (70) can in fact be regarded as a normal form for systems with a line of fixed points and a reflection symmetry (Fiedler et al., 2000). Their behaviour depends on the sign of PQ. If $PQ > 0$ then some solutions grow

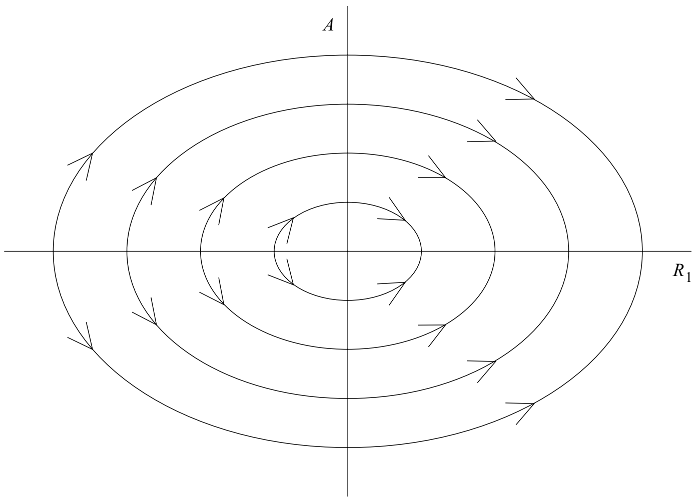

Fig. 10 Phase portrait of (69) and (70) in the case $Q < 0$, $P > 0$. All points on the R_1 axis are fixed points. The case $Q > 0$, $P < 0$ is the same but with the arrows reversed.

and become unbounded, indicating that terms of higher order need to be included. By contrast for $PQ < 0$, solutions are bounded, and since

$$\frac{\mathrm{d}}{\mathrm{d}\tau}(PA^2 - QR_1^2) = 0, \tag{71}$$

the trajectories are curves $PA^2 - QR_1^2 =$ constant, which are ellipses, if $PQ < 0$. In the case $Q < 0 < P$, the fixed points $A = 0$ with $R_1 < 0$ are unstable, and those with $R_1 > 0$ are stable, and the elliptical trajectories form heteroclinic orbits that link the unstable and stable fixed points, as shown in Fig. 10.

It is of interest to compute the sign of P from the formula (68), to determine whether the domain size increases or decreases as the pattern forms. For the Schnakenberg model with the growth law $F(u, v) = \alpha u - \beta v$, this calculation reveals that P is proportional to $3v_0^2 - 3\alpha u_0 - k^2$, so in general, the domain may grow or shrink. For the parameter values $p = 0.9$ and $q = 0.1$, as used in most of our simulations, $u_0 = 0.9$ and $v_0 = 1$, so $P \propto 3 - 2.7\alpha - k^2$. For the simulation shown in Fig. 7, the domain size is 1, so k is a multiple of π and $P < 0$. Hence the weakly nonlinear analysis is consistent with the numerical simulation showing decreasing domain size.

To compare the numerical simulations with the weakly nonlinear analysis and the phase portrait shown in Fig. 10, some further simulations of (22)–(25) were carried out closer to onset than those in Section 3.3. Fixing $\alpha = 0.1$ (and hence $\beta = 0.09$ to satisfy $\alpha u_0 = \beta v_0$) we see from Fig. 9 that the maximum value of d for which patterns can occur is near to 0.2 (in fact this value is 0.1973). Choosing to fix $d = 0.19$ and solving (54) for k, we find that the critical wavenumbers are 1.165 and 1.495 (so that the uniform state is unstable to patterns with wavenumbers between these values). Choosing $n = 2$ in (52), this gives critical values of R_0 as either

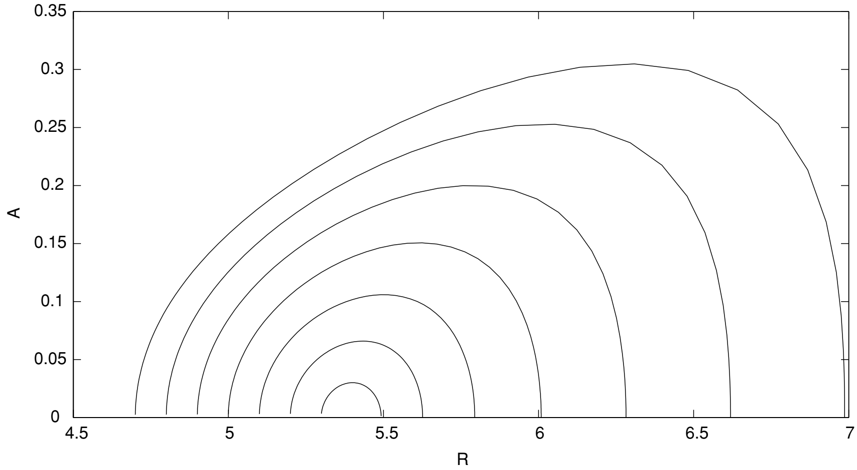

Fig. 11 Phase portrait obtained from seven numerical simulations of (22)–(25), plotting amplitude of the $\cos(2\pi\xi)$ mode against R, with trajectories running in the direction of increasing R. Parameter values: $p = 0.9$, $q = 0.1$, $d = 0.19$, $\alpha = 0.1$, $\beta = 0.09$, with $R(t = 0) = 4.7, 4.8, \ldots, 5.3$.

5.392 or 4.202. For these values of k, the above argument shows that $P > 0$, so the domain size increases as the pattern forms. For bounded solutions we therefore require $Q < 0$; this means that the growth rate must decrease as R increases, so we must choose the larger value for R_0, $R_0 = 5.392$.

A sequence of numerical simulations with initial values of R slightly below this value of R_0 is shown in Fig. 11. In each case the initial condition is a small random perturbation from u_0 and v_0, and the amplitude of u is plotted against R. In the vicinity of R_0, where the amplitude is small, the trajectories form nested ellipses, in agreement with the phase portrait in Fig. 10 predicted by the weakly nonlinear amplitude Eqs. (69) and (70). At larger amplitude, beyond the range of validity of the weakly nonlinear theory, the trajectories are no longer elliptical, but the picture remains qualitatively the same. This is to be expected since for $\alpha u_0 = \beta v_0$ the spatially uniform state is an equilibrium for any value of the domain size R. Further simulations confirmed that the full nonlinear system has the same $A \leftrightarrow -A$ symmetry as the amplitude equations.

The behaviour of the chemicals u and v is shown in Fig. 12 for the simulation with initial $R = 4.7$. In the initial phases, the amplitude $A(t)$ grows exponentially because R lies in the unstable band $4.202 < R < 5.392$, but there is no discernible change in R because R only increases quadratically with A. As A becomes larger, R starts to increase, because $P > 0$, until the growth rate of A becomes negative. A then decreases and the system ends up at the uniform state $A = 0$ with $R =$ constant. These simulations show that the amplitude Eqs. (69) and (70) provide a good description of the behaviour of the full PDEs for small-amplitude patterns when $\alpha u_0 = \beta v_0$ provided that $PQ < 0$.

We can generalise the amplitude Eqs. (69) and (70) in several ways. If d differs from the critical value given by (55) by an amount ϵd_1, then there is an order ϵ

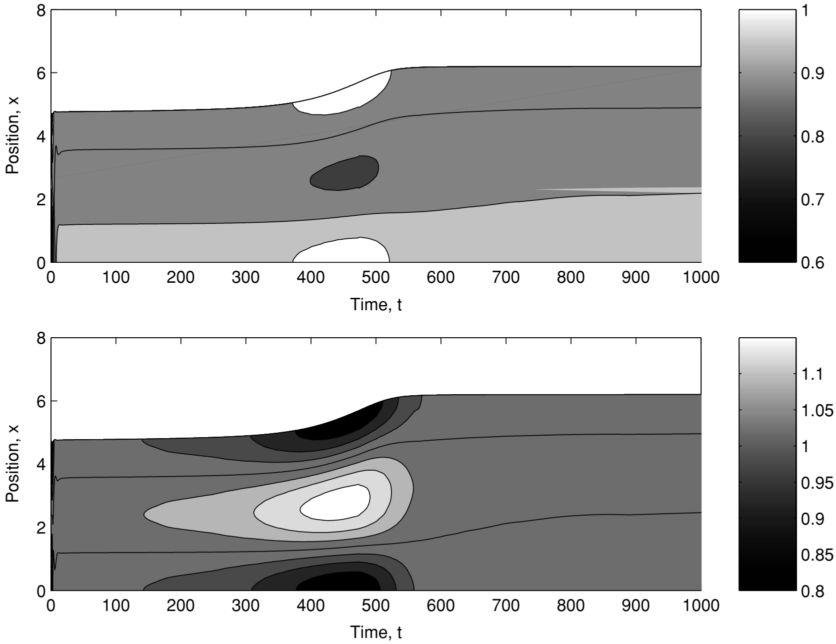

Fig. 12 Simulation results for u (*upper panel*) and v (*lower panel*) when $F(u, v) = \alpha u - \beta v$ and the chemicals interact via Schnakenberg kinetics. Parameter values: as per figure 11, with $u(x, t) = u_0 + 0.5\cos(\pi\xi)$, $v(x, t) = v_0$ and $R(t) = 4.7$ at $t = 0$. We note that for small time the kinetics are fast.

growth rate of A when $R_1 = 0$, so (69) will become

$$\frac{\mathrm{d}A}{\mathrm{d}\tau} = rA + QAR_1, \tag{72}$$

where r is proportional to d_1. This additional term has no effect on the dynamics other than to shift the origin of R_1, since we can define $R_1' = R_1 + r/Q$ and recover the original form (69), so the behaviour will be the same as shown in Fig. 10.

Similarly, we might allow $\alpha u_0 - \beta v_0$ to be nonzero, so that the domain grows even when there is no pattern. In this case (70) becomes

$$\frac{\mathrm{d}R_1}{\mathrm{d}\tau} = \mu + PA^2, \tag{73}$$

where the constant μ is proportional to $\alpha u_0 - \beta v_0$. This generalisation does lead to different dynamics, since there is no longer a line of fixed points along $A = 0$. If $\frac{\mu}{P} < 0$ there are just two fixed points at $A^2 = -\frac{\mu}{P}$, and if $PQ < 0$ these fixed points are centres. In this case the heteroclinic orbits in Fig. 10 are replaced by nested periodic orbits.

5. Conclusions

In this paper we have developed and analysed a theoretical model of pattern formation on a growing domain that places previous work (Crampin et al., 1999) in a more general context. The domain of interest represents a generic, one-dimensional tissue that consists of live cells whose rates of proliferation and death are regulated by local levels of two interacting, diffusible chemicals. The volume changes associated with the net rate of cell growth generate a local cell velocity and drive domain growth. As such our model combines previous moving boundary problems developed to describe the development of multicellular tumour spheroids in vitro (Byrne and Chaplain, 1997; Greenspan, 1976) with models of Turing systems (Gierer and Meinhardt, 1972; Murray, 1981; Turing, 1952). To illustrate how coupling domain growth to the chemical species affects the system we investigated the cases of exponential and chemically-controlled domain growth.

Our analysis of exponential domain growth extended previous work by Crampin et al. (1999) by investigating more thoroughly the impact on pattern formation of dilution effects due to domain growth. We showed that for large domain growth rates inclusion of the dilution terms is essential not only for correct pattern generation but also for ensuring that the amount of chemical in the domain is computed correctly (compare Figs. 2 and 3). We note also that the frequency-doubling phenomenon observed at slow growth rates is lost at high growth rates, regardless of whether dilution is included or not. As we have mentioned, it is well known that a uniform steady state which is linearly stable in the absence of diffusion, may be driven unstable by the inclusion of diffusion (Turing, 1952). We have shown that chemical dilution, caused by domain expansion, may further destabilize it. Hence we reiterate that retention of dilution effects is essential for correct pattern generation.

As mentioned above, real biological tissues consist of live cells and volume changes associated with cell birth and death generate velocity fields that drives domain growth (Alison and Sarraf, 1997; Jackson, 2002). Hence, our second case study involved coupling the evolution of the domain size to that of the chemicals. Numerical simulations of this nonuniform growth model reveal that the observed behaviour is strongly influenced by the system parameters and that there is a complex interaction between the chemical patterns and the evolving domain (compare Figs. 5–8). In order to gain insight into the way in which interactions between the diffusible chemicals and the evolving domain give rise to the range of behaviour reported by our numerics we performed a weakly nonlinear analysis on a generalised version of our model. This clearly demonstrates how the domain growth influences the critical diffusion coefficient (as a function of the wavenumber) at which spatial patterns may emerge. Also, with the wavenumber defined in terms of model parameters, the domain size at which spatial patterns appear depends on the chemical kinetics and the domain growth rate itself. We showed that the inclusion of chemical-dependent growth makes the uniform state more unstable to pattern formation, i.e. the region of (d, k) parameter space in which patterning is predicted increases (see Fig. 9). Analysis at higher order revealed how the pattern amplitude and domain size evolve over time. Indeed, the domain grows (or shrinks) as a quadratic function of the pattern amplitude.

The results presented in the paper are largely theoretical, our main aim being to present a mathematical framework for studying pattern formation on growing domains and to illustrate how domain growth may be influenced by (and influence) diffusible species present within the domain. In order to make the model more biologically meaningful it must be specialised to a particular tissue (and cell population) and candidate diffusible species known to influence tissue growth identified. The diffusible species of interest may be externally supplied nutrients or drugs, or cell-derived growth factors and proteins. For example, the cells and chemicals of interest could be epithelial cells, oxygen and the protein Wnt (Kuhnert et al., 2004; Pinto et al., 2003). Further analysis of such a specialised model may explain how mutations in other proteins such as APC that are known to interact with the Wnt signalling pathway may give rise to unwarranted (cancerous) expansion of the epithelial tissue (Fodde, 2001).

Other model modifications that are of interest include relaxing the no-flux boundary conditions to allow chemical transport across the domain boundary and allowing for multiple cell types (Pettet et al., 2001; Ward and King, 1997; Wein et al., 2003). We could also consider other spatial geometries, being mindful that extension to two or more spatial dimensions requires the introduction of a constitutive law to specify fully the velocity field (see Greenspan, 1976; Franks and King, 2003 for details).

In conclusion, the model presented in this paper provides a framework for studying pattern formation in growing tissues. Our analysis demonstrates that interactions between domain growth and the levels of diffusible species present in the tissue, as embodied in the local cell proliferation rate, can have a significant impact on both its size and chemical composition.

Acknowledgements

The authors thank Prof. O. Jensen at the Centre for Mathematical Medicine, University of Nottingham, for useful discussions whilst preparing this manuscript and gratefully acknowledge financial support from the EPSRC in the form of a studentship (AAN) and an advanced fellowship (HMB).

References

Alberts, B., Bray, D., Lewis, J., Raff, M., Roberts, K., Watson, J.D., 1994. Molecular Biology of the Cell. Garland Publishing, New York.

Alison, M.R., Sarraf, C.E., 1997. Understanding Cancer. Cambridge University Press, Cambridge, New York and Melbourne.

Benson, D.L., Maini, P.K., Sherratt, J.A., 1998. Unravelling the Turing bifurcation using spatially varying diffusion coefficients. J. Math. Biol. 37, 381–417.

Benson, D.L., Sherratt, J.A., Maini, P.K., 1993. Diffusion driven instability in an inhomogeneous domain. Bull. Math. Biol. 55, 365–384.

Breward, C.J.W., Byrne, H.M., Lewis, C.E., 2002. The role of cell–cell interactions in a two-phase model for avascular tumour growth. J. Math. Biol. 45, 125–152.

Byrne, H.M., Chaplain, M.A.J., 1995. Growth of nonnecrotic tumors in the presence and absence of inhibitors. Math. Biosci. 130, 151–181.

Byrne, H.M., Chaplain, M.A.J., 1997. Free boundary value problems associated with the growth and development of multicellular spheroids. Eur. J. Appl. Math. 8, 639–658.
Byrne, H.M., Chaplain, M.A.J., 1998. Necrosis and apoptosis: Distinct cell loss mechanisms in a mathematical model of avascular tumour growth. J. Theor. Med. 1, 223–235.
Byrne, H.M., Matthews, P.C., 2002. Asymmetric growth of models of avascular solid tumours: exploiting symmetries. IMA J. Math. Appl. Med. Biol. 19, 1–29.
Campbell, J.W., Pollack, I.F., 1997. Growth factors in gliomas: Antisense and dominant negative mutant strategies. J. Neuro-Oncol. 35, 275–285.
Casciari, J.J., Sotirchos, S.V., Sutherland, R.M., 1992. Mathematical modelling of microenvironment and growth in EMT6/Ro multicellular tumour spheroids. Cell Prolif. 25, 1–22.
Chaplain, M.A.J., 1996. Avascular growth, angiogenesis and vascular growth in solid tumours: The mathematical modelling of the stages of tumour development. Math. Comp. Mod. 23, 47–87.
Chaplain, M.A.J., Ganesh, M., Graham, I.G., 2001. Spatio-temporal pattern formation on spherical surfaces: Numerical simulation and application to solid tumour growth. J. Math. Biol. 42, 387–423.
Crampin, E.J., Gaffney, E.A., Maini, P.K., 1999. Reaction and diffusion on growing domains: Scenarios for robust pattern formation. Bull. Math. Biol. 61, 1093–1120.
Crampin, E.J., Hackborn, W.W., Maini, P.K., 2002. Pattern formation in reaction-diffusion models with nonuniform domain growth. Bull. Math. Biol. 64, 747–769.
Crank, J., 1984. Free and Moving Boundary Problems. Clarendon Press (Oxford University Press), Oxford.
Fiedler, B., Liebscher, S., Alexander, J.C., 2000. Generic Hopf bifurcation from lines of equilibria without parameters: I. Theory. J. Diff. Equat. 167, 16–35.
Fodde, R., 2001. Apc, signal transduction and genetic instability in colorectal cancer. Nat. Rev. Cancer 1, 55–67.
Franks, S.J., King, J.R., 2003. Interactions between a uniformly proliferating tumour and its surroundings: uniform material properties. Math. Med. Biol. 20, 47–89.
Gierer, A., Meinhardt, H., 1972. A theory of biological pattern formation. Kybernetik 12, 30–39.
Gray, P., Scott, S.K., 1983. Autocatalytic reactions in the isothermal, continuous stirred tank reactor. Chem. Eng. Sci. 38, 29–43.
Greenspan, H.P., 1976. On the growth and stability of cell cultures and solid tumours. J. Theor. Biol. 56, 229–242.
Grindrod, P., 1996. The Theory and Applications of Reaction-Diffusion Equations—Patterns and Waves of Oxford Applied Mathematics and Computing Science Series. Clarendon Press (Oxford University Press), Oxford.
Harrison, L.G., Kolář, M., 1988. Coupling between reaction-diffusion prepattern and expressed morphogenesis, applied to desmids and dasyclads. J. Theor. Biol. 130, 493–515.
Jackson, T.L., 2002. Vascular tumor growth and treatment: Consequences of polyclonality, competition and dynamic vascular support. J. Math. Biol. 44, 201–226.
Jones, A.F., Byrne, H.M., Gibson, J.S., Dold, J.W., 2000. A mathematical model of the stress induced during avascular tumour growth. J. Math. Biol. 40, 473–499.
Kondo, S., Asai, R., 1995. A reaction-diffusion wave on the skin of the marine angelfish *Pomacanthus*. Nature 376, 765–768.
Kuhnert, F., Davis, C.R., Wang, H.T., Chu, P., Lee, M., Yuan, J., Nusse, R., Kuo, C.J., 2004. Essential requirements for Wnt signalling in proliferation of adult small intestine and colon revealed by adenoviral expression of Dickkopf-1. Proc. Natl. Acad. Sci. USA 101, 266–271.
Lengyel, I., Epstein, I.R., 1991. Modelling of Turing structures in the chlorite iodide malonic acid starch reaction system. Science 251, 650–652.
Maini, P.K., Painter, K.J., Nguyen Phong Chau, H., 1997. Spatial pattern formation in chemical and biological systems. J. Chem. Soc. Faraday Trans. 93, 3601–3610.
Majack, R.A., 1987. Beta-type transforming growth factor specifies organizational behaviour in vascular smooth muscle cell cultures. J. Cell Biol. 105, 465–471.
Matthews, P.C., 1998. Hexagonal patterns in finite domains. Physica D 116, 81–94.
Murray, A., Hunt, T., 1993. The Cell Cycle. Oxford University Press, Oxford, New York, Toronto and Delhi.
Murray, J.D., 1981. A pre-pattern formation mechanism for animal coat markings. J. Theor. Biol. 88, 161–199.
Murray, J.D., 1993. Mathematical Biology, of Biomathematics Texts, vol. 19, 2nd edition. Springer-Verlag, Berlin and London.

Neubert, M.G., Caswell, H., Murray, J.D., 2002. Transient dynamics and pattern formation: reactivity is necessary for Turing instabilities. Math. Biosci. 175, 1–11.

Neville, A.A., 2003. Biomedical Modelling Incorporating Growth, PhD thesis, University of Nottingham, Nottingham, England.

Ouyang, Q., Swinney, H.L., 1991. Transition from a uniform state to hexagonal and striped Turing patterns. Nat. (Lond.) 352, 610–612.

Owen, M.R., Sherratt, J.A., 1999. Mathematical modelling of macrophage dynamics in tumours. Math. Mod. Meth. Appl. Sci. 9, 513–539.

Painter, K.J., Maini, P.K., Othmer, H.G., 1999. Stripe formation in juvenile *Pomacanthus* explained by a generalised Turing mechanism with chemotaxis. Proc. Natl. Acad. Sci. USA 96, 5549–5554.

Painter, K.J., Maini, P.K., Othmer, H.G., 2000. Development and applications of a model for cellular response to multiple chemotactic cues. J. Math. Biol. 41, 285–314.

Pettet, G.J., Please, C.P., Tindall, M.J., McElwain, D.L.S., 2001. The migration of cells in multicell tumor spheroids. Bull. Math. Biol. 63, 231–257.

Pinto, D., Gregorioff, A., Beghtel, H., Clevers, H., 2003. Canonical Wnt signals are essential for homeostasis of the intestinal epithelium. Genes Dev. 17, 1709–1713.

Santini, M.T., Rainaldi, G., Indovina, P.L., 2000. Apoptosis, cell adhesion and the extracellular matrix in the three-dimensional growth of multicellular tumor spheroids. Crit. Rev. Oncol. Hemat. 36, 75–87.

Schnakenberg, J., 1979. Simple chemical reaction systems with limit cycle behaviour. J. Theor. Biol. 81, 389–400.

Sherratt, J.A., Chaplain, M.A.J., 2001. A new mathematical model for avascular tumour growth. J. Math. Biol. 43, 291–312.

Turing, A.M., 1952. The chemical basis of morphogenesis. Phil. Trans. Roy. Soc. Lond. B237, 37–72.

Varea, C., Aragon, J.L., Barrio, R.A., 1997. Confined Turing patterns in growing systems. Phys. Rev. E 56, 1250–1253.

Ward, J.P., King, J.R., 1997. Mathematical modelling of avascular-tumour growth. IMA J. Math. Appl. Med. Biol. 14, 39–69.

Ward, J.P., King, J.R., 1999. Mathematical modelling of avascular-tumour growth II: Modelling growth saturation. IMA J. Math. Appl. Med. Biol. 16, 171–211.

Wein, L.M., Wu, J.T., Kirn, D.H., 2003. Validation and analysis of a mathematical model of a replication and competent oncolytic virus for cancer treatment: implications for virus design and delivery. Cancer Res. 63, 1317–1324.